Subbarrier fusion of ^{16}O + ^{147,149}Sm

D. E. DiGregorio, M. diTada, D. Abriola, M. Elgue, A. Etchegoyen, M. C. Etchegoyen,
J. O. Fernández Niello, A. M. J. Ferrero, S. Gil, A. O. Macchiavelli,
A. J. Pacheco, and J. E. Testoni

Departamento de Física-TANDAR, Comisión Nacional de Energía Atómica, 1429 Buenos Aires, Argentina

P. R. Silveira Gomes

Instituto de Física da Universidade Federal Fluminense, Niteroi, Brazil

V. R. Vanin, R. Liguori Neto, and E. Crema

Instituto de Física da Universidade de São Paulo, São Paulo, Brazil

R. G. Stokstad

Nuclear Science Division, Lawrence Berkeley Laboratory, Berkeley, California 94720

(Received 8 August 1988)

Fusion cross sections have been measured for ^{16}O + ^{147,149}Sm at bombarding energies in the range 61 MeV $\leq E_{lab}(^{16}O) \leq$ 75 MeV by off-line observation of x rays emitted in the radioactive decay of Yb isotopes and their daughters. The fusion excitation functions are similar to those of the adjacent even Sm isotopes. It appears, therefore, that the odd valence neutrons do not have any unusual influence on the subbarrier enhancement of σ_{fus} in these systems. The x-n distributions of the evaporation residues were also determined. The nuclear deformation parameters β_2 deduced for the odd and even Sm isotopes using Wong's model establish a smooth systematic behavior of β_2 with target collectivity. Fusion cross sections for ^{16}O with all the stable Sm isotopes are tabulated.

I. INTRODUCTION

The cross sections for the fusion of heavy ions at energies below the Coulomb barrier can be orders of magnitude larger than the predictions of one-dimensional barrier penetration models.[1-6] Experimental and theoretical studies of these enhancements have revealed the important role played by the nuclear structure of the colliding nuclei. Different factors that have been explicitly considered in order to explain the behavior of the fusion excitation functions are permanent deformation,[2,3] zero-point oscillations of the nuclear shape,[7] formation of a neck,[8,9] and nucleon transfer.[10,11] More recently, the coupled channel formalism has been used to describe both static and dynamic effects in the collision.[12-15]

From an experimental standpoint, an important indication of the role played by the shape degrees of freedom in the subbarrier enhancement came from the study of the fusion of ^{16}O with various even samarium isotopes.[2,3] The samarium nuclei are known to exhibit a wide range of deformation, from the spherical, semimagic ^{144}Sm to the well-deformed ^{154}Sm. The use of a doubly magic projectile such as ^{16}O was considered to be important in order to be able to isolate effects that could, in principle, be attributed to the different deformations of the different target nuclei. The results obtained in Ref. 3 clearly showed that larger deformation (as found in the heavier isotopes of samarium) corresponded to larger subbarrier enhancements of the fusion cross sections. The study of the ^{16}O + ^{144}Sm (Ref. 2) not only confirmed the trend previously observed for the rest of the even samarium iso-

topes, it also provided the *basic* barrier parameters needed to undertake a more quantitative description of the phenomenon.

In spite of the large number of different systems studied in recent years, experimental data for systems with odd nuclei as one of the reaction partners are still relatively rare.[6] In this paper the study of fusion cross sections at energies in the vicinity of the interaction barrier was extended to include the reactions of ^{16}O with the two stable odd samarium isotopes, ^{147}Sm and ^{149}Sm. The purpose of this investigation was twofold; first it might prove possible to observe effects due to the presence of valence nucleons, in excess of those expected from the deformation of the core. Second, the study of these two nuclei is expected to provide information on the behavior of the deduced nuclear deformation parameters in the whole mass range. This is particularly important for the case of ^{147}Sm, which is the closest stable nucleus to the semimagic ^{144}Sm.

We also report the fusion cross sections for ^{16}O + ^{144}Sm, for which only a short account of the experiment has appeared, and then provide a tabular summary of all the recent fusion cross sections measured for ^{16}O + Sm.[2,3]

II. THE EXPERIMENT

The fusion cross sections are determined by observation of delayed x-rays emitted by the evaporation residues produced in the reaction and collected in a catcher foil. This technique has been described in Ref. 3. We mention

here those details peculiar to these experiments.

The measurements were carried out using beams of ^{16}O ions provided by the 20UD tandem accelerator at the Tandar Laboratory in Buenos Aires. These beams, with laboratory energies between 61 and 75 MeV, were used to bombard targets of isotopically enriched ^{147}Sm (98.0%) and ^{149}Sm (97.4%) with thicknesses of 40 μg/cm^2 and 125 μg/cm^2, respectively, evaporated onto thin carbon backings. The absolute energy of the ^{16}O beam has an uncertainty of $\pm$0.5%, which has been determined by calibrating the 90° analyzing magnet of the tandem accelerator with an improved proton recoil method.[16]

The Yb evaporation residues were trapped in an aluminum foil of 800 μg/cm^2, which was placed 2 mm behind the samarium target. The thickness of the catcher foil was sufficient to stop the evaporation residues while letting through the products of the reaction of ^{16}O with the oxygen impurity in the target, with the carbon of the target backing, and with the aluminum of the same catcher foil. During selected runs a second catcher foil was located behind the first one in order to verify that none of the evaporation residues was lost.

Two silicon surface-barrier detectors were placed at $\pm$30° to the beam and at a distance of 31 cm from the target for monitoring the elastic and inelastic scattering of ^{16}O with the samarium isotopes. Since the cross section for elastic scattering (including unresolved low-lying states) is given by the Rutherford formula at this angle, and the solid angle of the monitor detector is known, it is possible to obtain an absolute measurement of the cross section independent of the target thickness and the integrated beam current. The intensity of the beam during the bombardments, typically 20–100 electrical nanoamperes, was recorded by multiscaling in one-minute intervals the integrated current in the Faraday cup.

Following irradiations of about 100–120 min, the catcher foils were removed from the scattering chamber and placed in front of a 5 cm^3 Ge planar x-ray detector. The time between the end of the irradiation and the start of the counting was typically 3–5 min; thus, activities with half-lives shorter than 1 or 2 min were not observed. X-ray spectra were recorded automatically at various time intervals during several hours. Figures 1 and 2 show typical photon spectra associated with the decay of Yb and its daughters obtained for ^{16}O$+^{149}$Sm at E_{lab}=75 MeV and at 63 MeV, respectively. The cross sections at these two energies differ by 2 orders of magnitude. The x-ray detector had an energy resolution of 480 eV (FWHM) at 50 keV, which allowed separation of the $K_{\alpha 1}$, $K_{\alpha 2}$ lines of the x-rays of Tm, Er, Ho, and Dy. The absolute photopeak efficiency of the detector was determined using a set of calibrated sources that were carefully mounted in the same geometry as the catcher foils. This efficiency was 3.7$\pm$0.12 % at an energy of 40–60 keV. In addition, corrections were made for summing effects due to the simultaneous detection of more than one photon. Electronic deadtime was negligible.

Areas of the $K_{\alpha 1}$, $K_{\alpha 2}$ lines were obtained by fitting with shapes having a Gaussian plus an exponential tail, and using shape parameters obtained from the spectra themselves. The error in the determination of the peak
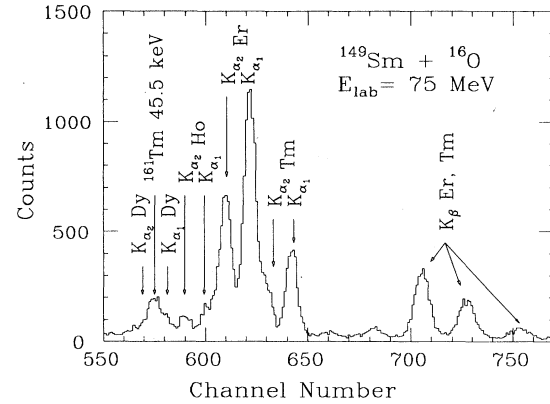

FIG. 1. Offline K x-ray energy spectra obtained for radioactive decay of Yb nuclei and their daughters produced after a 100 min bombardment of ^{149}Sm with ^{16}O at E_{lab}=75 MeV. The counting time began 9 min after the end of the bombardment and lasted for 5 min.

areas was estimated to be about 3–5 %. K_β lines were not analyzed.

In order to check the experimental technique, measurements of fusion cross sections using ^{16}O beams and an isotopically enriched target of ^{148}Sm (98.0 %) were performed and the results were compared with those of Ref. 3.

III. THE TIME DEPENDENCE OF X-RAY COUNT RATES

Examples of the measured K_α x-ray count rates from thulium, erbium, holmium, and/or dysprosium residues as a function of the time are shown in Figures 3 and 4 for ^{16}O$+^{149}$Sm at bombarding energies of 75 MeV and 63 MeV, respectively. Taking into account the contribution
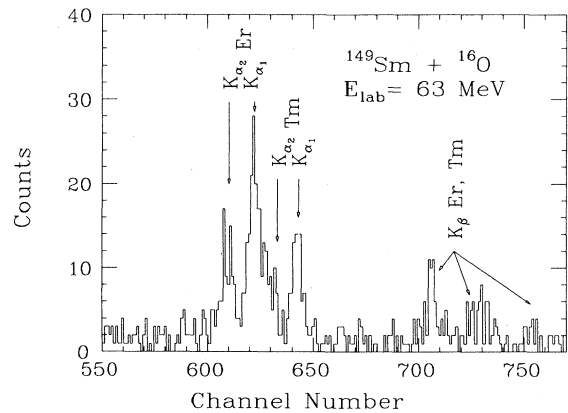

FIG. 2. Off-line K x-ray energy spectra obtained for radioactive decay of Yb nuclei and their daughters produced after a 128 min bombardment of ^{149}Sm with ^{16}O at E_{lab}=63 MeV. The counting time began 15 min after the end of the bombardment and lasted for 5 min.
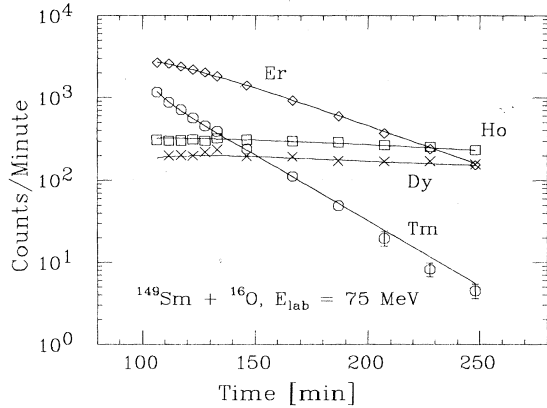
FIG. 3. The K_α x-ray count rates from thulium, erbium, holmium and dysprosium as a function of the time after the start of the bombardment of ^{149}Sm with ^{16}O at $E_{lab}=75$ MeV. The curves are simultaneous fits to the data using known half-lives and absolute K_α x-ray intensities as described in the text.

FIG. 5. The deduced relative intensities of different mass chains, expressed as a percentage of the fusion cross sections, as a function of bombarding energy for ^{16}O + ^{144,147,148,149}Sm. The solid curves are statistical model calculations performed using the computer code PACE (Ref. 23).

from different decay chains, σ_A, the intensity of the K_α x-rays in the counting interval defined by t_I and t_F, divided by its length $t_I - t_F$, can be calculated as follows:

$$A_Z(t_I, t_F) = \sum_A \sigma_A W_{Z,A} F_{Z,A}(T_{1/2}, t_I, t_F) . \qquad (1)$$

The function $F_{Z,A}(T_{1/2}, t_I, t_F)$ is proportional to the integral between t_I and t_F of the activity for the decay of the nucleus (Z, A). $T_{1/2}$ are the known half-lives and $W_{Z,A}$ are the numbers of K_α x-rays produced per decay of each isotope in each mass chain: both were obtained from Ref. 17. The absolute K_α x-ray intensities can be deduced from normalized level schemes by evaluating the K_α vacancies produced by internal conversion of the individual nuclear transitions and by electron capture to
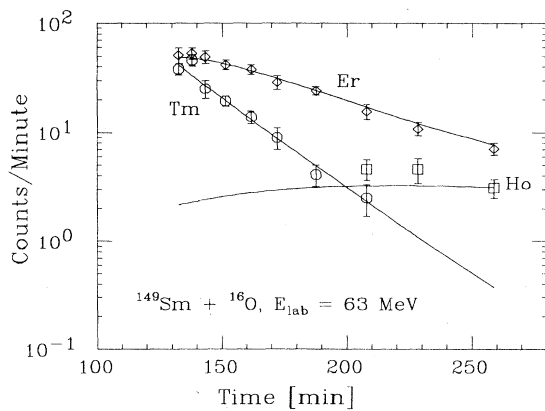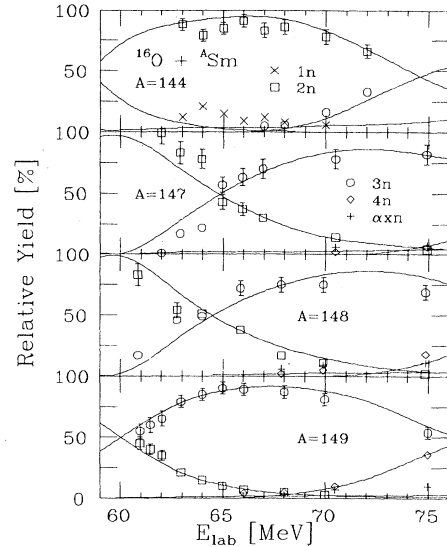

FIG. 4. The K_α x-ray count rates from thulium, erbium, and holmium as a function of the time after the start of the bombardment of ^{149}Sm with ^{16}O at $E_{lab}=63$ MeV. The curves are simultaneous fits to the data using known half-lives and absolute K_α x-ray intensities as described in the text.

levels of a daughter nucleus. For those nuclei far from stability line where the decay schemes are not known, a nominal estimate was necessary. However, these nuclei have little influence on the determination of the cross sections.

In comparing the experimental data with the calculated intensities, the evaporation residue cross sections, σ_A, were taken as adjustable parameters in a least-squares procedure. These calculations were performed using the code XRAY.[18] The values of σ_A thus obtained were used to determine the fusion cross sections for the different systems as follows:

$$\sigma = \sum_A \sigma_A \qquad (2)$$

The full curves in Figs. 3 and 4 are simultaneous fits of the activities for the first three generations of the decay chains (thulium, erbium and holmium). When possible the fourth generation (dysprosium) was also included in the fit. The contributions of isomeric states with half-lives of several minutes, such as are present in $A = 160$ and $A = 158$, were treated explicitly as additional decay chains. The possibility of charged particle emission, either proton or α particle, has also been included. However, only the α-xn channels are relevant, especially at the higher energies measured, since it is very difficult to distinguish experimentally between a $3n$ or $p2n$ process because the half-lives of the first members of the decay chains are too short for the time scale of the present measurements. Fission of the compound nucleus was estimated to be negligible in the range of masses and bombarding energies involved in these reactions.

IV. RESULTS

The different isotopic contributions, expressed as a percentage of the fusion cross sections, deduced for the systems ^{144,147,148,149}Sm+^{16}O at several bombarding energies are displayed in Fig. 5 and are listed in Table I. The $1n$, $2n$, $3n$, $4n$ and α-xn excitation functions show the expected systematic behavior with bombarding energy, as evidenced by the agreement with a statistical model calculation (curves). These calculations are described in Sec. VI.

The fusion cross sections obtained using expression (2) are listed in Table II. The laboratory bombarding energies given in Tables I and II correspond to the energy at the center of the target. There are several sources of error that contribute to the uncertainty in the fusion cross sections. Among the systematic errors the most important are those coming from the absolute normalization based on Rutherford scattering, and the absolute efficiency of the x-ray detector. They were estimated to be 9% and 5%, respectively. Among the errors that are partly systematic and partly random in nature, the most

important are those of the coefficients $W_{Z,A}$ of expression (1), which are known to ±10%. Since we fit simultaneously the x-ray yields from at least three generations, for each of at least two decay chains, the combined error is reduced significantly. The error on the cross section arising from the statistical uncertainty in the peak areas and the fitting of the decay curves was calculated by examining the dependence of chi-square per degree of freedom on the value of σ. These errors were typically 5%. By summing in quadrature the different sources of error just mentioned (excluding beam energy) an overall error of approximately 12% in the fusion cross sections was calculated. The errors are higher (15–20%) at the three lowest bombarding energies, where the counting statistics were lower.

We have also tabulated the fusion cross sections for ^{16}O and the other isotopes of Sm as given in Refs. 2 and 3. The cross sections for ^{16}O+^{148}Sm were measured in the present work in order to have a precise determination of the relative shapes of the excitation functions for the odd and adjacent even isotopes of Sm. The agreement be-

TABLE I. xn and α-xn distributions (%).

	E_{lab} (MeV)	$1n$ (%)	$2n$ (%)	$3n$ (%)	$4n$ (%)	α-xn (%)
^{16}O+^{144}Sm[a]	72.0	1	66	33		
	70.0	6	78	16		
	68.0	8	86	6		
	66.0	9	91	0		
	65.0	15	85	0		
	64.0	21	79	0		
	63.0	12	88	0		
^{16}O+^{147}Sm	74.9		4	82	6	8
	70.5		14	78	2	6
	66.9		30	70	0	0
	65.9		37	63	0	0
	65.0		43	57	0	0
	64.0		78	22	0	0
	62.9		83	17	0	0
	62.0		99	1	0	0
^{16}O+^{148}Sm	74.9		2	69	18	11
	69.9		11	75	5	9
	67.8		17	75	2	6
	65.9		28	72	0	0
	64.0		51	49	0	0
	62.8		54	46	0	0
	60.9		83	17	0	0
^{16}O+^{149}Sm	75.0		0	54	36	10
	70.5		3	81	10	7
	68.0		5	87	5	3
	66.0		7	89	0	0
	65.0		10	90	0	0
	64.0		15	85	0	0
	63.0		21	79	0	0
	62.0		35	65	0	0
	61.5		40	60	0	0
	61.0		45	55	0	0

[a]From Ref. 2.

tween the present results (solid squares) and those of Ref. 3 (circles) is generally good, as can be seen in Fig. 6. However, at the higher bombarding energies the present values are about 15% higher. These differences arise from the inclusion in the present analysis of the α-xn channels.

V. ANALYSIS OF CROSS SECTIONS AND DEFORMATION PARAMETERS

The experimental results for the fusion cross sections of the systems $^{16}O+^{147,148,149}Sm$ are summarized in Fig. 7. This figure shows *reduced* fusion cross sections versus *reduced* center-of-mass energies. These *reduced* quantities are defined in such a way that geometric effects due to small variations in nuclear radii and masses are removed. The dimensionless *reduced* fusion cross section,

σ_{red}, is defined by

$$\sigma_{\text{red}} = \sigma_{\text{fus}}/(\pi R_B^2) \tag{3}$$

and the dimensionless *reduced* center-of-mass energy is defined by

$$E_{\text{c.m.}}^{\text{red}} = E_{\text{c.m.}}/V_B \tag{4}$$

where the radius R_B and the Coulomb barrier V_B are given by

$$R_B = r_B(A_1^{1/3} + A_2^{1/3}), \tag{5}$$

$$V_B = 1.44 Z_1 Z_2/r_e(A_1^{1/3} + A_2^{1/3}) \tag{6}$$

with $r_B = 1.32$ fm and $r_e = 1.54$ fm.[2] The squares, diamonds, and circles correspond to the experimental data for ^{147}Sm, ^{148}Sm, and ^{149}Sm, respectively, measured in the

TABLE II. Cross sections for fusion of ^{16}O with the stable isotopes of Sm.

	E_{lab} (MeV)	σ_{fus} (mb)		E_{lab} (MeV)	σ_{fus} (mb)
$^{16}O+^{144}Sm^a$	72.0	309.0 ±31.0	$^{16}O+^{149}Sm$	75.0	460.0 ±55.0
	70.0	164.0 ±16.0		70.0	191.0 ±23.0
	68.0	74.4 ±7.5		68.0	127.0 ±15.0
	67.0	39.9 ±4.0		66.0	56.6 ±6.8
	66.0	13.6 ±1.4		64.9	32.6 ±3.9
	65.0	4.3 ±0.6		63.9	15.4 ±1.8
	64.0	0.99±0.15		63.0	7.0 ±1.1
	63.0	0.27±0.04		62.0	3.0 ±0.5
				61.5	1.9 ±0.4
				61.0	0.63±0.13
$^{16}O+^{147}Sm$	74.9	404.0 ±48.0			
	70.5	210.0 ±25.0	$^{16}O+^{150}Sm^b$	75.0	440.0 ±44.0
	66.9	69.0 ±8.0		70.0	243.0 ±24.0
	65.9	47.3 ±5.7		67.5	117.0 ±12.0
	65.0	27.3 ±3.3		65.0	38.4 ±3.8
	64.0	7.6 ±1.2		63.8	20.2 ±2.0
	62.9	2.8 ±0.4		62.5	7.75±0.8
	62.0	0.52±0.1		61.2	2.22±0.22
				60.0	0.472±0.047
$^{16}O+^{148}Sm$	74.9	463.0 ±56.0			
	69.9	213.0 ±26.0	$^{16}O+^{152}Sm^b$	75.0	462.0 ±46.0
	67.8	120.0 ±14.0		70.0	213.0 ±21.0
	65.9	42.2 ±5.1		64.9	· 43.9 ±4.4
	64.0	13.9 ±2.1		63.7	24.4 ±2.4
	62.8	4.7 ±0.7		62.4	11.7 ±1.2
	60.9	0.50±0.1		61.2	4.4 ±0.44
				59.9	1.06±0.11
$^{16}O+^{148}Sm^b$	75.0	404.0 ±40.0	$^{16}O+^{154}Sm^b$	75.1	430.0 ±43.0
	70.0	183.0 ±18.0		70.1	235.0 ±24.0
	67.5	89.4 ±9.0		67.5	134.0 ±14.0
	65.0	27.0 ±2.7		65.0	55.8 ±5.6
	63.8	10.7 ±1.1		63.8	29.4 ±2.9
	62.5	3.13±0.31		62.5	15.3 ±1.5
	61.5	0.721±0.72		61.3	6.24±0.62
	60.0	0.115±0.012		60.0	2.21±0.22

[a]From Ref. 2.
[b]From Ref. 3.
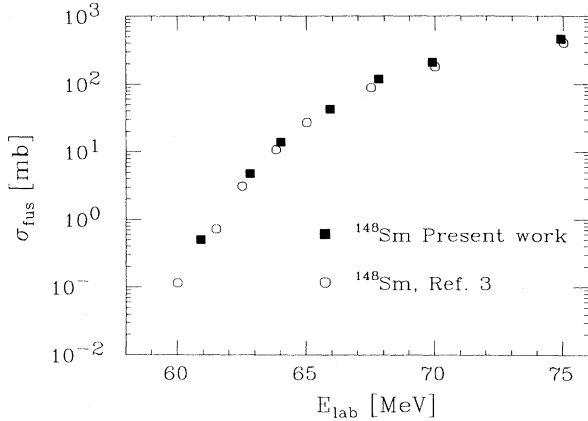
FIG. 6. Measured fusion cross sections as a function of bombarding energy for ^{16}O+^{148}Sm. Full squares correspond to the present measurements and circles correspond to data taken from Ref. 3.

FIG. 8. Experimental and theoretical *reduced* fusion cross sections for ^{16}O with the odd isotopes divided by the corresponding cross sections for ^{16}O with ^{148}Sm, as a function of *reduced* center-of-mass energies.

present work. The differences in the excitation functions for ^{147,148,149}Sm can be seen more clearly if the experimental *reduced* cross sections are normalized to those for ^{148}Sm. This is done in Fig. 8. (Since the cross sections for the different Sm isotopes have not been measured at exactly the same value of $E_{c.m.}^{red}$, each experimental data point for ^{147}Sm and ^{149}Sm has been normalized by interpolating between two closest data points for ^{148}Sm using the slope of the theoretical calculation.)

To analyze the fusion excitation functions of ^{16}O+^{147,148,149}Sm we use a one-dimensional barrier-penetration model that includes deformation effects (Wong's model).[19] Following the approach of Ref. 2, the σ_{fus} for the different systems were calculated by using the above values of V_B and R_B, taking the curvature of the potential $\hbar\omega = 3.9$ MeV, and leaving the nuclear deformation of the target nucleus β_2 as the only free parameter.
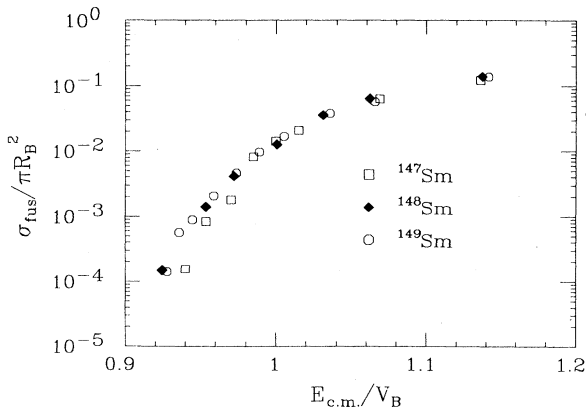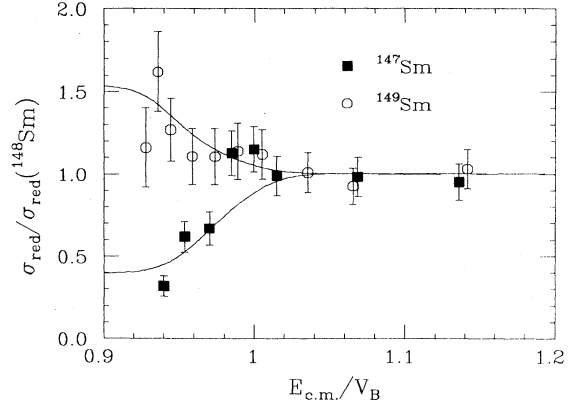

FIG. 7. *Reduced* fusion cross sections versus *reduced* center-of-mass energies for ^{16}O+^{147,148,149}Sm. The squares, diamonds, and circles correspond to the experimental data for ^{147}Sm, ^{148}Sm, and ^{149}Sm, respectively, measured in the present work.

With this fitting procedure the β_2 values were deduced for all the different samarium isotopes. The solid curves in Fig. 8 are the theoretical cross sections for the two odd samarium isotopes divided by the corresponding values for ^{148}Sm.

In order to check possible effects due to the unpaired nucleons, it is necessary to make a detailed analysis of the behavior of the deduced quadrupole deformation parameter β_2. The values of β_2 deduced by fitting cross sections with the model of Ref. 19 will depend on any effects that produce a subbarrier enhancement, even those effects that are not directly related to shape degrees of freedom. In this case, one may expect differences in values of the deformation parameters deduced from the fusion data using the one-dimensional barrier-penetration model and the corresponding values obtained from other sources, such as the reduced $E2$ transition probabilities $B(E2)$.[20,21] Since the collective features of the nucleus relevant to fusion enhancement and relevant to the determination of the $B(E2)$ are similar but not necessarily identical, it is important to examine the systematic behavior of β_2 rather than the absolute values for a given isotope.

Figure 9 shows the results for the quadrupole deformation parameter β_2 deduced in this work for the odd Sm isotopes from the fits using Wong's model, together with those obtained in Ref. 2 for the even Sm isotopes. These values of β_2 (solid squares) are plotted versus the corresponding values obtained from the experimental reduced $E2$ transition probabilities $B(E2)$, which were calculated for each isotope using the prescription given in Refs. 20 and 22. In particular, for the odd isotopes this was done as follows: the quadrupole deformation parameter β_2 was obtained through the formula

$$\beta_2 = \sqrt{5\pi/9}\,\frac{Q_0}{ZR_0^2}\,, \tag{7}$$

where $R_0 = 1.2\,A^{1/3}$ fm. The intrinsic quadrupole moment Q_0 was calculated using the expression,

$$B(E2;KI_1 \rightarrow KI_2) = \frac{5}{16\pi}e^2Q_0^2\langle I_1 K 20 | I_2 K \rangle^2 , \quad (8)$$

which takes into account the presence of the extra nucleon that is assumed to occupy a given Nilsson level in the ground-state configuration. The experimental $B(E2)$ values for the stretched $E2$ transition between the excited state $\frac{11}{2}^-$ and the ground state $\frac{7}{2}^-$ were used for both nuclei ^{147}Sm and ^{149}Sm.[21] The value of K was determined from an inspection of the Nilsson diagram for this mass region under the requirement that the deduced values of K and β_2 be self-consistent. Of the possible values of K ($\frac{1}{2}, \frac{3}{2}, \frac{5}{2}, \frac{7}{2}$), the self-consistent results are $K = \frac{3}{2}$, $\beta_2 = 0.13$ for ^{147}Sm and $K = \frac{5}{2}$, $\beta_2 = 0.156$ for ^{149}Sm.

The comparison in Fig. 9 shows that, although the relation between the parameters obtained using the one-dimensional barrier-penetration model and those obtained from $B(E2)$ values is not linear, all the isotopes, including the odd ones, fall on a rather smooth curve. This indicates that, within the sensitivity of this method, the odd nucleons do not have a pronounced effect on fusion cross sections below the barrier. Moreover, this behavior (trend) is relatively independent of the values adopted for $\hbar\omega$ and for the β_2 value of ^{144}Sm, which were taken from Ref. 2. There, Wong's model was used to fit the experimental excitation function of ^{16}O + ^{144}Sm (taken as the reference system) leaving $\hbar\omega$ and β_2 as free parameters. Values of $\hbar\omega = (3.9\pm0.2)$ MeV and β_2 (^{144}Sm) $= 0.00\pm0.03$ were obtained. Another approach consists in taking for ^{144}Sm the value of $\beta_2 = 0.088$ obtained from the $B(E2)$ value and then fit the experimental points leaving $\hbar\omega$ as the only free parameter. In this case a value of $\hbar\omega = 3.2$ MeV was obtained. The analysis of the ^{16}O with all the samarium isotopes then gives a new set of values for β_2, (circles in Fig. 9) which show the

same trend. Regarding this dependence, the β_2 values obtained from fusion increase very slowly for the heaviest samarium isotopes, in contrast with the rapid rise observed starting from ^{144}Sm. Note that the existence of this rapid rise is confirmed by the inclusion of the new data point corresponding to ^{147}Sm.

VI. STATISTICAL MODEL CALCULATIONS OF THE *x-n* DISTRIBUTIONS

We have made statistical model calculations using the code PACE (Ref. 23) to analyze the measured *x-n* distributions and to estimate the relative importance of the fission decay mode. This version of the code PACE uses the fission barriers that incorporate the effects of the finite range of the nuclear force and the diffuseness of the nuclear surface.[24] In order to predict the competition between fission and particle evaporation, it is necessary to specify the level density parameters a_n and a_f, which determine the level densities at the ground state and the saddle point, respectively. For the ratio a_f/a_n we have used the same value as given in Ref. 25, namely $a_f/a_n = 1.0$, with $a_n = A/8.5$ [MeV^{-1}]. The reduced gamma-transition strengths used in all our calculations were 0.025, 0.01, 9.0, and 1.2 W.u. for the $E1$, $M1$, $E2$, and $M2$ transitions, respectively. The spin distributions in the compound nucleus were obtained from Wong's model with parameters adjusted to fit the measured fusion cross section.[4] Very good agreement between the experimental values of the relative yields and the statistical model calculations is obtained as shown (full lines) in Fig. 5 for the systems ^{16}O + ^{144,147,148,149}Sm. Furthermore, similar calculations describe very well the relative yields for ^{16}O with the other stable samarium isotopes ^{150,152,154}Sm taken from Ref. 3 (not shown in Fig. 5). In all the cases studied the contribution of the fission channel is less than 1% at the highest bombarding energy used.

VII. SUMMARY

We have measured the fusion cross sections for ^{16}O with ^{147,149}Sm at energies above and below the Coulomb barrier. These measurements complete our experimental study of the influence of nuclear deformation in the fusion of ^{16}O with all stable samarium isotopes. The *x-n* distributions for ^{16}O + ^{144,147,148,149}Sm were well described by statistical model calculations. In comparison with the energy dependence of σ_{fus} for the even-even Sm isotopes, the odd Sm isotopes do not show any unusual effects that might be ascribed to the presence of an unpaired neutron. An analysis based on a one dimensional barrier-penetration model that includes the effect of nuclear deformation shows that the behavior of the values of β_2 deduced from σ_{fus} follows the systematics established by the even-even isotopes, i.e., the quadrupole deformation parameters obtained for the odd isotopes fit well with the trend of values determined for the even isotopes. This trend shows that the onset of strong collectivity occurs rapidly as nucleons are added to ^{144}Sm.
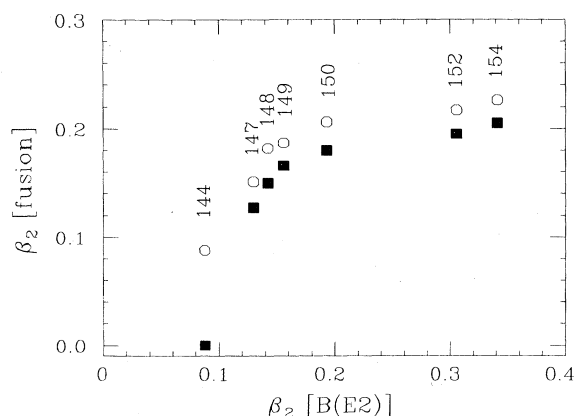

FIG. 9. β_2 values deduced from fusion vs β_2 values deduced from experimental reduced $E2$ transition probabilities $B(E2)$ for the different samarium isotopes. The nucleus ^{144}Sm was taken as the reference system. Full squares correspond to β_2 values deduced using $\hbar\omega = 3.9$ MeV and β_2 (^{144}Sm) $= 0.00\pm0.03$, following the approach of Ref. 2. Circles correspond to β_2 values deduced using $\hbar\omega = 3.2$ MeV and β_2 (^{144}Sm) $= 0.088$ obtained from the $B(E2)$ value (see the text).

[1] M. Beckerman, Phys. Rep. **129**, 145 (1985).

[2] D. E. DiGregorio, J. O. Fernández Niello, A. J. Pacheco, D. Abriola, S. Gil, A. O. Macchiavelli, J. E. Testoni, P. R. Pascholati, V. R. Vanin, R. Liguori Neto, N. Carlin Filho, M. M. Coimbra, P. R. S. Gomes, and R. G. Stokstad, Phys. Lett. B **176**, 322 (1986).

[3] R. G. Stokstad, Y. Eisen, S. Kaplanis, D. Pelte, U. Smilansky, and I. Tserruya, Phys. Rev. Lett. **41**, 465 (1978); Phys. Rev. C **21**, 2427 (1980).

[4] S. Gil, R. Vandenbosch, A. J. Lazzarini, D.-K. Lock, and A. Ray, Phys. Rev. C **31**, 1752 (1985).

[5] M. Beckerman, M. Salomaa, S. Sperduto, H. Enge, J. Ball, A. DiRienzo, S. Gazes, Y. Chen, J. D. Molitoris, and M. Hai-Feng, Phys. Rev. Lett. **45**, 1472 (1980); M. Beckerman, J. Ball, H. Enge, A. Sperduto, S. Gazes, A. DiRienzo, and J. D. Molitoris, Phys. Rev. C **23**, 1581 (1981); M. Beckerman, M. Salomaa, S. Sperduto, J. D. Molitoris, and A. DiRienzo, *ibid.* **25**, 837 (1982).

[6] S. J. Skorka, A. M. Stefanini, G. Fortuna, R. Pengo, W. Meczynsky, G. Montagnoli, A. Tivelli, S. Beghini, C. Signorini, and P. R. Pascholati, Z. Phys. A **328**, 355 (1987).

[7] H. Esbensen, Nucl. Phys. A**352**, 147 (1980).

[8] L. C. Vaz, J. M. Alexander, and G. R. Satchler, Phys. Rep. **69C**, 374 (1981).

[9] U. Jahnke, H. H. Rossner, D. Hilsher, and E. Holub, Phys. Rev. Lett. **48**, 17 (1982).

[10] R. A. Broglia, C. H. Dasso, S. Landowne, and G. Pollarolo, Phys. Lett. **133B**, 34 (1983).

[11] R. A. Broglia, C. H. Dasso, and S. Landowne, Phys. Rev. C **32**, 1426 (1985).

[12] C. H. Dasso and S. Landowne, Phys. Lett. B **183**, 141 (1987); Comput. Phys. Commun. **46**, 187 (1987).

[13] C. H. Dasso, S. Landowne, and A. Winther, Nucl. Phys. A**405**, 318 (1983); A**407**, 221 (1983); A**432**, 495 (1985).

[14] J. Q. Wu and G. F. Bertsch, Nucl. Phys. A**457**, 401 (1986).

[15] M. J. Rhodes-Brown and P. Braun-Munzinger, Phys. Lett. **136B**, 19 (1984).

[16] A. M. J. Ferrero, A. Garcia, S. Gil, A. Etchegoyen, M. diTada, A. J. Pacheco, D. Abriola, D. E. DiGregorio, M. C. Etchegoyen, J. O. Fernández Niello, A. O. Macchiavelli, and J. E. Testoni (unpublished).

[17] At. Data Nucl. Data Tables **29** (1983).

[18] A. J. Pacheco, D. E. DiGregorio, J. F. Fernández Niello, and M. Elgue, Comput. Phys. Commun. (in press).

[19] C. Y. Wong, Phys. Rev. Lett. **31**, 766 (1973).

[20] At. Data Nucl. Data Tables **36** (1987).

[21] C. Garrett, J. R. Leigh, and G. D. Dracoulis, Nucl. Phys. A**262**, 137 (1976).

[22] A. Bohr and B. R. Mottelson, *Nuclear Structure* (Benjamin, New York, 1974) Vol. II.

[23] A. Gavron, Phys. Rev. C **21**, 230 (1980).

[24] A. Sierk, private communication; A. J. Krappe, J. R. Nix and A. Sierk, Phys. Rev. C **20**, 992 (1979).

[25] K. T. Lesko, W. Henning, K. E. Rehm, G. Rosner, J. P. Schiffer, G. S. Stephans, B. Zeidman, and W. S. Freeman, Phys. Rev. C **34**, 2155 (1986).